ACS OMEGA

http://pubs.acs.org/journal/acsodf

Article

Development of a New Ternary Al_2O_3–HAP–Pd Catalyst for Diethyl Ether and Ethylene Production Using the Preferential Dehydration of Ethanol

Chaowat Autthanit, Nutdanai Likitpiriya, Piyasan Praserthdam, and Bunjerd Jongsomjit*

Cite This: *ACS Omega* 2021, 6, 19911–19923

Read Online

ACCESS | Metrics & More | Article Recommendations | Supporting Information

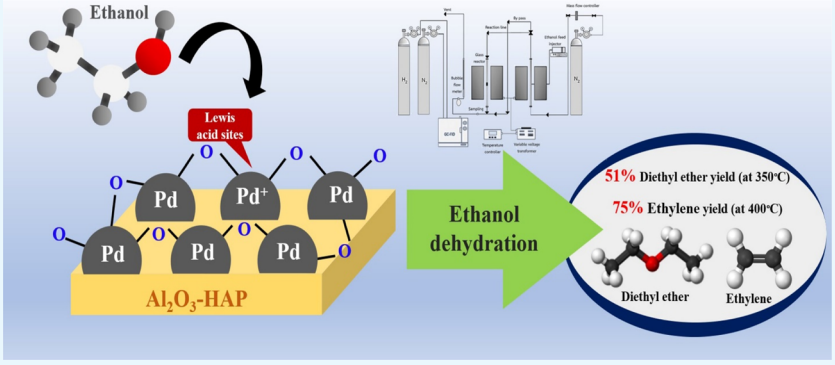

ABSTRACT: This study aims to convert ethanol to higher value-added products, particularly diethyl ether and ethylene using the catalytic dehydration of ethanol. Hence, the gas-phase dehydration of ethanol over Al_2O_3-HAP catalysts as such and modified by addition of palladium (Pd) in a microreactor was evaluated. The commercial Al_2O_3–HAP catalyst was first prepared by the physical mixing method, and then, the optimal ratio of the Al_2O_3–HAP catalyst (2:8 by wt %) was impregnated with Pd to develop a new functional catalyst to alter surface acidity. Based on the results, the combination of Al_2O_3 and HAP catalysts generated significant quantities of weak acid sites which demonstrates an enhancement in catalytic activity. In addition, Pd modification in the optimal composition ratio of the Al_2O_3–HAP catalyst extremely increased the amount of weak acid sites as well as weak acid density due to the synergistic effect between the Pd and Al_2O_3–HAP catalyst that are supposed to suggest the active sites in the reaction. Among all catalysts, the Al20-HAP80-Pd catalyst displayed brilliant catalytic performance in the course of diethyl ether yield (ca. 51.0%) at a reaction temperature of 350 °C and ethylene yield (ca. 75.0%) at a reaction temperature of 400 °C having an outstanding stability under time-on-stream for 10 h. This is recognized to the combination of the effects of weak acid sites (Lewis acidity), small amount of strong acid sites, and structural characteristics of the catalytic materials used.

1. INTRODUCTION

The continuous increase in energy demand, as well as the need to decrease greenhouse gas emissions resulting from the usage of fossil fuels, led to a significant increase in research on renewable energy sources.[1] Bio-ethanol obtained by biomass fermentation is one of the crucial raw materials in the global shift from fossil-based resources to renewable ones.[2] For this reason, catalytic reactions of ethanol to higher value-added products such as hydrogen, diethyl ether, ethylene, 1-butanol, aldehydes, and so forth have been extensively investigated due to its sustainability.[3,4] Among the secondary intermediates potentially obtainable by converting ethanol, diethyl ether and ethylene can be obtained by catalytic ethanol dehydration. Basically, there are two conceivable reaction pathways for ethanol dehydration: intramolecular and intermolecular reaction pathways.[5] The former is an endothermic reaction (high reaction temperature, ca. 350–500 °C) that favors ethylene formation, while the latter suggests an exothermic reaction (low reaction temperature, ca. 150–350 °C) that renders diethyl ether formation.[6] Also, acetaldehyde can be produced by ethanol dehydrogenation as a side reaction. Homogenous catalysts exhibit advantages in terms of activity and stability due to their good solubility in reaction media. However, homogeneous catalysts are difficult to separate and recover from the reaction mixture, resulting in increasing economic cost, environmental pollution, and corrosion. Thus, the heterogeneous catalyst represents a very attractive system

Received: May 30, 2021
Accepted: July 16, 2021
Published: July 26, 2021

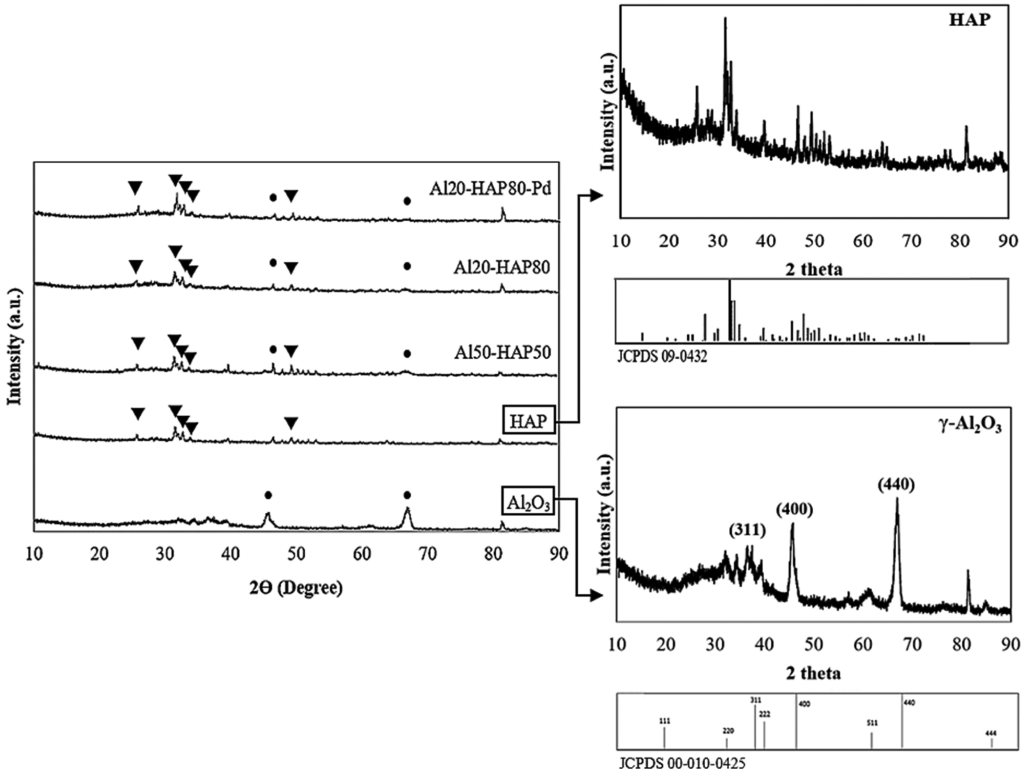

Figure 1. XRD patterns for all catalysts (● Al_2O_3 and ▼ HAP).

for obtaining bio-based and/or specific product because the reaction can be carried out as a continuous gas-phase process and catalyst separation problems are avoided.[2] Industrially, ethanol dehydration is carried out over solid acid catalysts with HZSM-5 zeolite and alumina (Al_2O_3) being the most commonly applied and thus used as benchmark catalysts.[7−9] In addition, amorphous silica-alumina,[10] transition-metal oxides,[11] phosphoric acid[12] and silica-supported heteropoly acids[5] can be named among other commonly studied catalysts. Nevertheless, the selective synthesis of diethyl ether and ethylene on solid acid catalyst with extremely high conversion, selectivity, and yield, especially with lower reaction temperature and stability, still needs further developments.

The selection of the catalyst depends on the products desired in the conversion of ethanol. Alumina is an active catalyst in the ethanol conversion, and depending on the reaction temperature, the product distribution can be directed toward diethyl ether and ethylene.[13] For example, Doheim et al.[14] investigated that Al_2O_3 doped with Na_2O and Mn_2O_3 followed by heating at 500 °C can improve the ethanol conversion (ca. 97%) at a reaction temperature of 300 °C. Feng et al.[15] investigated ethanol dehydration to ethylene on a mesoporous γ-Al_2O_3 catalyst prepared by a precipitation method and thereafter hydrothermal treatment method, showing that the surface area of the γ-Al_2O_3 catalyst had a great influence on ethanol conversion and ethylene selectivity at the same reaction temperature. Cosimo et al. revealed that Lewis acid site-Brønsted basic site pairs of different strengths on Al_2O_3 and mixed oxide ($MgO-Al_2O_3$) catalysts were required for the conversion of ethanol to ethylene and diethyl ether. Phung and Busca.[10] prepared $SiO_2-Al_2O_3$ catalysts by different procedures. The results demonstrated that ethanol conversion occurred on strong acid sites (Brønsted acid sites) together with weak acid sites (Lewis acid sites), which were more selective for diethyl ether and ethylene at suitable reaction conditions. However, many research works have stated that the intrinsic acidity of the Al_2O_3 support, especially the strong acid sites on the catalysts, can favor undesirable reactions that result in coke formation.[16−18] Therefore, an innovative idea is to decrease the amount of strong acid sites (Brønsted acid sites) and/or generate more weak acid sites (Lewis acid sites) which favors catalytic activity while reducing coke deposition on the catalyst surface.

To test these ideas, common methods to alter the strong acidity of Al_2O_3 to weak acid sites are the addition of basic catalysts to its surface. Hydroxyapatite [$Ca_{10}(PO_4)_6(OH)_2$, HAP] is naturally found in a major composition of skeleton, especially in bone and teeth.[19] Characteristics of the HAP catalyst depend on the Ca/P ratio including substitution of component ions. It shows active area with both of acidic and basic sites in a single-crystal lattice, which are crucial property for dehydration reaction.[20,21] For instance, Tsuchida et al.[22,23] studied the HAP catalyst in ethanol dehydration reaction. The results indicated that the reaction temperature and contact time led to enhancing various products such as ethylene, diethyl ether, 1,3-butadiene, butanol, olefins, propylene, aromatic, and so forth. Rahmanian and Ghaziaskar[19] studied the conversion of ethanol over $AlPO_4$/HAP catalysts with a (Ca + Al)/P molar ratio of 1.62 at high pressure and temperature (supercritical conditions). At these conditions, diethyl ether selectivity (ca. 96%) and diethyl ether yield (ca. 75%) were obtained. Hence, it is of interest to develop a combination of Al_2O_3 and HAP as a catalyst in dehydration of ethanol, but research including other metals and/or noble metals is still inadequate. From previous works in our laboratory,[4,24,25] it showed that the palladium (Pd) played a crucial role in ethanol dehydration, which depends on the reaction temperature. This is because the effect of Pd

https://doi.org/10.1021/acsomega.1c02818
ACS Omega 2021, 6, 19911−19923

Table 1. Characteristics of all Supports and Catalysts

catalysts	BET surface area (m^2/g)[a]	pore volume (cm^3/g)[b]	pore size (nm)[b]	amount of element on surface[c] (wt %) Ca	P	Al	O	Pd	Pd content (wt %)[d]	crystalline size (nm)[e]
Al_2O_3	13.5	0.3	5.6			64.3	35.7			22.3
HAP	1.2	0.1	10.3	37.6	22.9		39.5			26.1
Al50-HAP50	5.1	0.1	6.3	16.5	16.1	21.9	45.5			21.4
Al20-HAP80	2.2	0.2	6.4	25.4	17.0	13.7	43.9			21.8
Al20-HAP80-Pd	3.1	0.1	6.7	24.3	18.4	16.7	38.6	2.0	0.38	18.3

[a]Determined from the BET method. [b]Determined from the BJH adsorption method. [c]Determined from EDX analysis. [d]Determined from ICP analysis. [e]Calculated from XRD using the Scherrer equation.

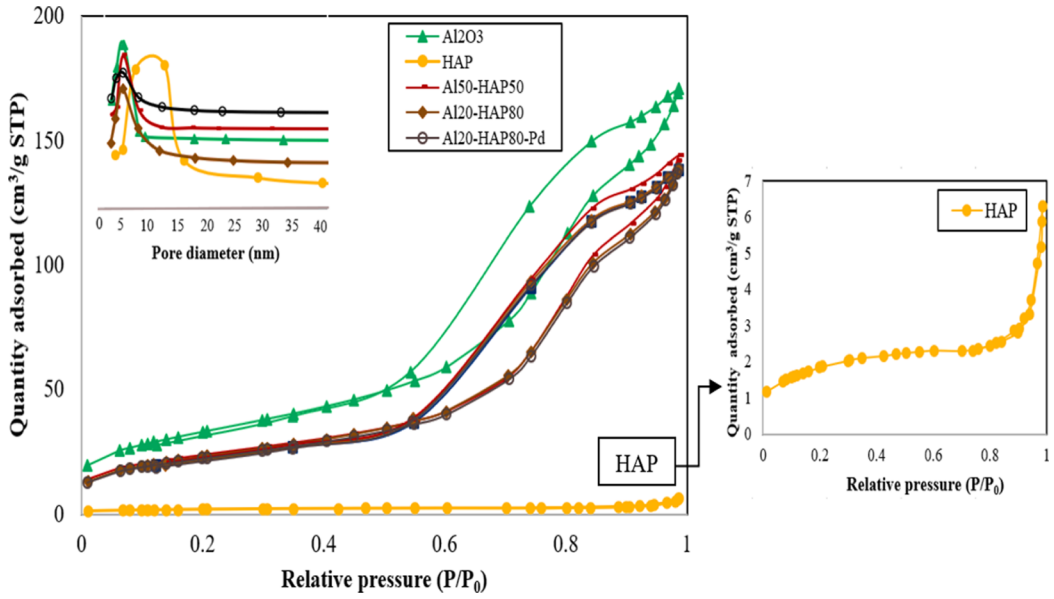

Figure 2. N_2 adsorption−desorption isotherms and PSD of all catalysts.

modification on the catalytic activity can be attributed to the increased amount of weak acid sites (Lewis acid sites). Hence, Pd is still added to elucidate the reasons for enhanced activity of the mixed Al_2O_3 and HAP catalysts. However, to the best knowledge of the authors, there are no detailed accounts of the catalytic performance for ethanol dehydration on the different composition ratios of Al_2O_3−HAP catalysts with Pd modification.

With this aim, the work reported here was performed to investigate the Al_2O_3 catalyst that were physically mixed with the HAP catalyst for ethanol dehydration. In addition, the optimal catalyst is now being focused on developments of noble Pd with their properties, stability, and performance in enhancing the catalytic reaction of ethanol dehydration to higher value-added products, especially diethyl ether and ethylene. The modified catalysts were then characterized by X-ray powder diffraction (XRD), N_2 physisorption, scanning electron microscopy−energy dispersive X-ray (SEM−EDX) spectroscopy, inductively coupled plasma (ICP), NH_3-TPD, and thermogravimetric analysis (TGA). A possible mechanism for ethanol dehydration is also proposed based on the results presented here.

2. RESULTS AND DISCUSSION

2.1. Catalyst Characterization. XRD analysis was carried out in order to describe the crystal structure and phase of the bulk catalysts. The XRD patterns of all different catalysts are displayed in Figure 1. The characteristic sharp peaks of the bare Al_2O_3 catalyst are located at 2θ values of 37° (311 reflection), 46° (400 reflection), and 67° (440 reflection) which is in agreement with the database standard for gamma-alumina structure JCPDS file no. 00-010-0425 (face-centered cubic structure) in the International Centre for Diffraction Data (ICDD) database.[26] The bare HAP catalyst flourished sharp peaks at 26, 30, 32, 33, and 49°, which is confirmed by the existence of the main diffraction peaks of hydroxyapatite identified based on JCPDS file no. 09-0432.[27] Furthermore, other mixing catalysts exhibited both the sharp peaks at 25−35, 46, and 67°, representing the crystallite structure of hydroxyapatite and alumina. No additional phases were detected in these mixing catalysts except a very small shift of the XRD patterns. Nevertheless, the peak of Pd was not observed due to the small loading of Pd metal and/or the very small size of crystallites (<3−5 nm) that are highly dispersed thoroughly in the Al20-HAP80 catalyst.

Based on the XRD data, the average crystallite size is usually obtained by calculating the full width at half-maximum and the Scherrer's equation, such as in refs 28 and 29 (Table 1). The average crystallite size of bare Al_2O_3 and bare HAP are 22.3 nm and 25.1 nm, whereas those of Al50-HAP50, Al20-HAP80, and Al20-HAP80-Pd catalysts are calculated as 21.4, 21.8 and 18.3 nm, respectively. The decrease in the crystallite size is due to the presence of HAP as well as the incorporation of Pd, which prevent the fusion of Al_2O_3 particles. Thus, the HAP

https://doi.org/10.1021/acsomega.1c02818
ACS Omega 2021, 6, 19911−19923

catalyst and metallic Pd helps to avoid the particle agglomeration and maintain the particle size smaller for Al50-HAP50, Al20-HAP80, and Al20-HAP80-Pd catalysts.

The Brunauer–Emmett–Teller (BET) surface area, average pore volume, and average pore size diameter of all catalysts are presented in Table 1. The bare Al_2O_3 possesses a BET surface area of 13.5 m^2 g^{-1}, a pore volume of 0.3 cm^2 g^{-1}, and a pore diameter of 5.6 nm. When increasing the amount of HAP, the BET surface area decreases due to the progressive blocking of pores by the HAP catalyst inside Al_2O_3 pore channels, particularly at higher HAP contents. However, after Pd is incorporated into the Al20-HAP80 catalyst, the BET surface area and pore volume of the catalyst did not show any significant change, suggesting that a small amount of Pd oxide nanoparticle was dispersed thoroughly on the Al20-HAP80 catalyst. Moreover, the average pore diameter ranged from 5.6 to 10.3 nm within the boundary of mesoporous values.

Figure 2 represents the N_2 physisorption isotherms and Barrett–Joyner–Halenda (BJH) pore size distribution (PSD) curves (the inset in Figure 2) of all catalysts. The analysis of shapes of the isotherms for all studied catalysts shows that they have the mesoporous structure. According to the IUPAC classification, all catalysts submit type IV isotherms, and the hysteresis loops can be classified into two types, that is, H1 indicating the existence of cylindrical pores and H3 (only bare HAP) related to some amount of slit-shape pores. For all different catalysts except the bare HAP catalyst, their N_2 uptake increased sharply over the relative pressure (P/P_0) of 0.5–0.9, due to the capillary condensation of N_2 within the uniform mesopores.[30] In the corresponding high P/P_0, the course of the isotherm is quite steep with respect to the pressure axis which indicates a large size of pores of cylindrical shape.[31] Therefore, the hysteresis loop of the bare HAP catalyst at $P/P_0 \approx 0.9$ in a wide range of pressures is horizontal which is due to the occurrence of slit pores.[32] Furthermore, the obtained PSD curves confirm that the pore sizes were in the range of 2–50 nm assigned to the mesoporous structure.

The SEM images of all catalysts are displayed in Figure 3. The morphology of the bare Al_2O_3 catalyst was quasi-spherical shape with a rough surface and their average particle size ranging from 0.3 to 0.5 μm, as well as the occurrence of very small intergranular pores. In the case of bare HAP, it was observed that the big grains are composed by small particles with oval shapes, agglomerated between them. The addition of HAP in Al_2O_3 catalysts (Al50-HAP50 and Al20-HAP80) show a fine-grained morphology with low intergranular porosity, composed of irregular-shaped grains. Similar SEM images were reported by de Lima et al.[33] After Pd was loaded into the Al20-HAP80 catalyst, it can be observed that there was only a slight change in the morphology of the catalyst. The morphology of all mixed Al_2O_3–HAP catalysts was smaller than bare Al_2O_3 having the average particle size less than 0.3 μm, indicating that the incorporation of HAP inhibited Al_2O_3 grain growth, reducing intergranular porosity, and hence, locally enhancing densification of the mixed Al_2O_3–HAP catalysts.

Elemental analysis of surfaces in SEM is performed using EDX, which measures the energy and intensity distribution of X-ray signals produced by the electron beam striking the surface of the catalyst samples. The distribution of Al and O in a particular region, as shown in Supporting Information, Figure S1, confirms the existence of alumina. Also, the dense distribution of Ca and P in Supporting Information, Figure S2, with meagerly disturbed oxygen confirms the existence of

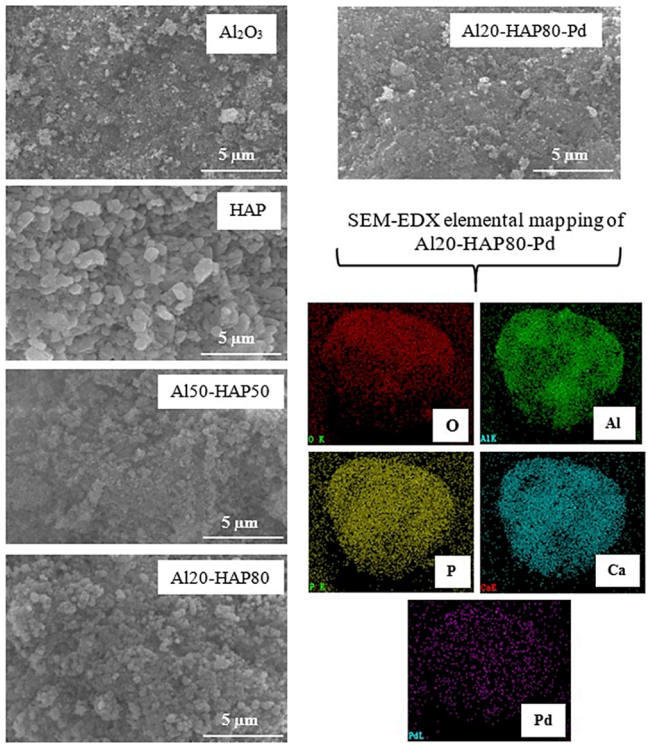

Figure 3. SEM micrographs of all catalysts and typical EDX for O, Al, Si, P, Ca, and Pd mapping (Al20-HAP80-Pd).

HAP. The elemental mapping of all Al_2O_3–HAP catalysts, as shown in Supporting Information, Figures S3 and S4, represents the microstructures of Al_2O_3 and HAP separately, which is evident that no other intermediate compounds are formed. Furthermore, the elemental mapping of the Al20-HAP80-Pd catalyst (Figure 3) indicated the ubiquitous presence of O, Al, P, Ca, and Pd at areas of differential concentration. The Pd distribution corresponds well to the Al, P, and Ca distributions, confirming the substitution of the Pd ions into the Al_2O_3–HAP lattice.[34] The elemental analysis from EDX analysis is summarized in Table 1, for the relative quantities of calcium, phosphorus, aluminum, oxygen, and palladium in each catalyst. In addition, ICP measurement was also performed to determine the bulk Pd loading. It can be seen that the Pd content at bulk (ICP) was at 0.38 wt % for the Al20-HAP80-Pd catalyst. Nevertheless, the elemental concentration from the EDX analysis, which is a surface analysis, provides an analysis depth of approximately 50 nm from the typical external granule, and shows therefore only a part of the whole analytical information; this is in total contrast to ICP analysis, which shows an average results in the catalyst sample.[35] Thus, the Pd content on the catalyst surface (EDX) is higher than Pd content in bulk measured by the ICP technique. This is consistent with our previous work[24,25] reported that Pd concentration obtained from EDX analysis was higher than those detected by the ICP technique.

The amount of surface acidity of all catalysts was examined by NH_3-TPD between 150 and 600 °C. Figure 4a–c shows the corresponding TPD profiles, distribution of acid sites, and distribution of acid density, respectively, while Table 2 assembles the amount of NH_3 desorbed (μmol NH_3 g^{-1} cat.) and acid density (μmol m^{-2}) for all different catalysts. There are mainly three desorption ranges in the TPD profiles: the desorption peak at a lower temperature below 300 °C is

https://doi.org/10.1021/acsomega.1c02818
ACS Omega 2021, 6, 19911–19923

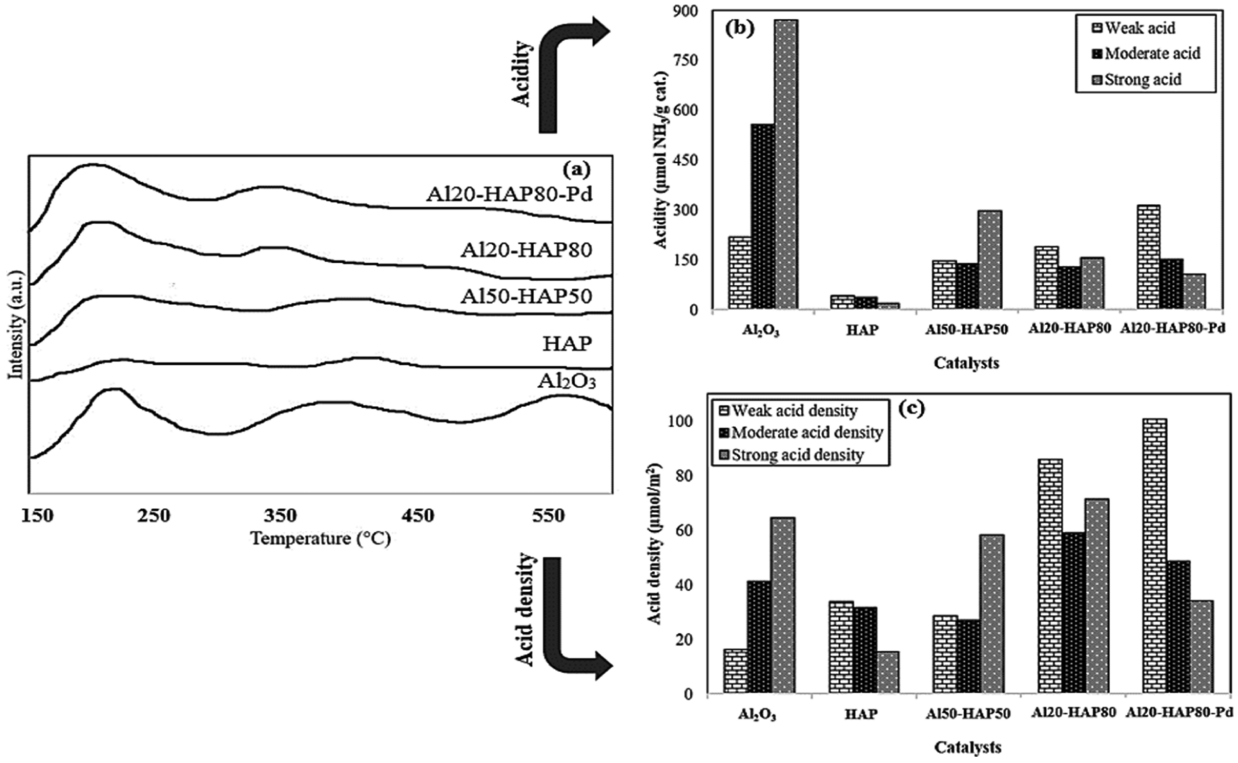

Figure 4. NH_3-TPD profiles (a), distribution of acid sites (b), and distribution of acid density (c) of all different catalysts.

Table 2. Amount of Surface Acidity and Acid Density of Catalysts Obtained by NH_3-TPD[a]

	acidity (μmol NH_3 g^{-1} cat.)				acid density (μmol/m^2)			
catalysts	weak	moderate	strong	total	weak	moderate	strong	total
Al_2O_3	219.6	556.7	871.3	1647.6	16.3	41.2	64.5	122.0
HAP	40.7	37.9	18.6	97.3	33.9	31.6	15.5	81.0
Al50-HAP50	146.6	137.3	297.9	611.9	28.7	26.9	58.4	114.0
Al20-HAP80	189.2	129.9	156.8	475.9	86.0	59.0	71.3	216.3
Al20-HAP80-Pd	312.7	151.4	105.5	569.6	100.9	48.8	34.0	183.7

[a]Acid density = number of acid sites/BET surface area.

attributed to weak acid sites; the second one at a medium temperature between 300 and 450 °C is assigned to moderate acid sites; and the third one at a high temperature above 450 °C is ascribed to strong acid sites.[36,37] The sum of all the three acid sites measured by the total ammonia desorbed gives the total acidity of the catalysts. The bare Al_2O_3 catalyst displays the largest total surface acidity maybe due to the high surface area as well as the high physical adsorption of NH_3 in the framework of the Al_2O_3 catalyst.[38] It is notable that with increase in the amount of HAP catalysts, the TPD profiles was shifted toward lower temperature which means that there was a loss in both moderate and strong acid sites with significant increase in the weak acid sites, indicating that the addition of HAP can facilitate the formation of weak acid sites. This is due to introduction of HAP that resulted in the synergistic interaction between Al−OH groups in the structure of Al_2O_3 (strong acid sites) and Ca^{2+} ions as well as the high coordination number of Ca^{2+} ions in the structure of HAP (strong basic sites), as pointed out by Gao et al.[39] Also, the incorporation of HAP into Al_2O_3 catalysts leads to the formation of calcium aluminate phases [such as $CaO(Al_2O_3)_6$, $CaAl_4O_7$, $Ca_3Al_2O_6$, $Ca_5Al_6O_{14}$, and $CaAl_2O_4$], probably generates the formation of weak acid sites on the expense of strong acidity.[40] After the impregnation of the active Pd (0.5 wt %) on the Al20-HAP80 catalyst, Al−HAP species interact with the active Pd species to form the [Al−HAP]−Pd^+−O bond, resulting in the formation of weak acid sites. Thus, the Al20-HAP80-Pd catalyst showed the highest weak acid site of 312.7 μmol NH_3 g^{-1} cat. Besides, the decrease in the number of the strong acid sites is observed due to the loading of Pd ions. This indicated that these strong acid sites represent Brønsted acid sites, which are reduced due to ion exchange of the Pd ion with H^+ ions. This also described that weak acid sites obtained by NH_3-TPD are representative of Lewis acid sites (Lewis sites which are electron deficient).[41] By integrating the area under desorption peaks, the amount of NH_3 desorbed, particularly associated to the amounts of weak acid sites from the catalysts decreases according to the following order: Al20-HAP80-Pd (312.7 μmol NH_3 g^{-1} cat.) > Al_2O_3 (219.6 μmol NH_3 g^{-1} cat.) > Al20-HAP80 (189.2 μmol NH_3 g^{-1} cat.) > Al50-HAP50 (146.6 μmol NH_3 g^{-1} cat.) > HAP (40.7 μmol NH_3 g^{-1} cat.) (see Table 2). Likewise, the amount of moderate acid sites were also small and increased with the impregnation of Pd. It is generally recognized that weak acid sites (Lewis acid sites) play an important role in ethanol dehydration to diethyl ether and ethylene, whereas the oligomerization and

https://doi.org/10.1021/acsomega.1c02818
ACS Omega 2021, 6, 19911−19923

Scheme 1. Conceptual Surface Acidity Model of the Al_2O_3−HAP Catalyst with Pd Modification

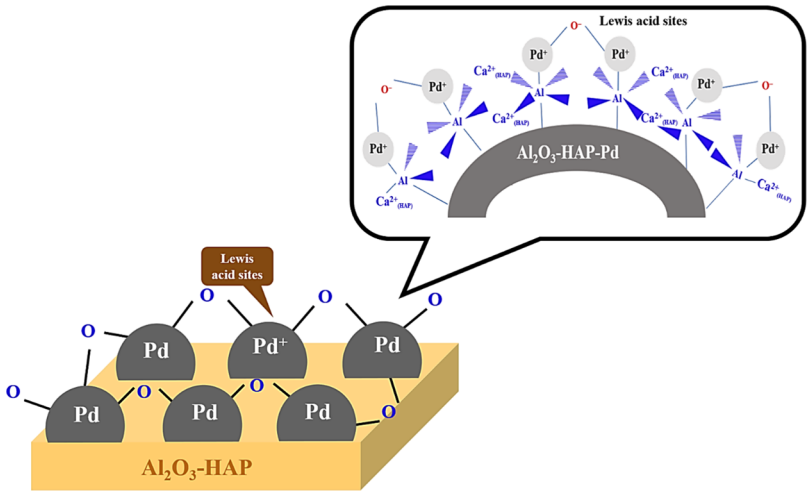

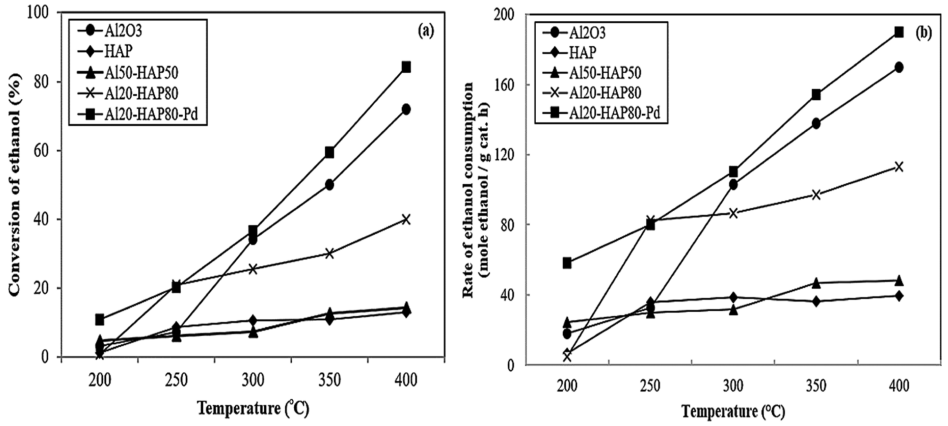

Figure 5. Ethanol conversion (a) and reaction rate (b) of all different catalysts. Reaction condition: 0.05 g catalyst, ethanol flow rate = 1.45 mL/h, at atmosphere pressure, WHSV = 22.9 ($g_{ethanol}$ g_{cat}^{-1}) h^{-1}.

alcohol transformation to higher hydrocarbons takes place in the strong acid sites (Brønsted acid sites).[42] Additionally, the amount of acid density on a solid catalyst is typically expressed as the number or mmol of acid sites per unit surface area (BET). In spite of the decrease of total acid sites on all modified catalysts when compared with the unmodified catalyst (bare Al_2O_3), these catalysts show high values of acid density expressed as μmoles of NH_3 per surface unit, due to their low specific BET surface areas. The Al20-HAP80-Pd catalyst demonstrated the highest density of weak acid sites (100.9 μmol m^{-2}) among all different catalysts. Besides, the strength of acid sites as well as high acid density are crucial for improving the conversion and selectivity toward target products.[43] This crucial characterization will be used to elucidate the catalytic behaviors for all different catalysts during the ethanol dehydration reaction. The conceptual surface acidity model of the Al_2O_3−HAP catalyst with Pd modification is summarized in Scheme 1. In fact, the Al−OH group of the bare Al_2O_3 catalyst exhibited the Brønsted acid sites property, but its acidity is very weak, which however possess a very strong acid site character on the surface. Then, after mixing with the HAP catalyst (Ca^{2+} ions and/or species), Ca^{2+} substitute the OH groups located in adjacent six-coordinated aluminum atoms and, therefore, can alter the strong acid sites of bare Al_2O_3 to form (Al−Ca_{HAP}^{2+})−O bonds, which can be generated as weak acid sites (Lewis acid sites). In addition, it is obvious that modification of Pd on the Al_2O_3−HAP catalyst led to [Al−Ca_{HAP}^{2+}]−Pd^{+}−O bonds, which indicates a larger amount of Lewis acid sites.

2.2. Catalytic Evaluation of Ethanol Dehydration. Normally, the ethanol can be transformed into value-added chemical products including diethyl ether and ethylene based on the reaction temperature by catalytic dehydration over the solid acid catalysts. Zhang et al.[44] claimed that the formation of diethyl ether and ethylene is thermodynamically favored at 150−350 and 350−500 °C, respectively. The experiment was performed with the same catalyst weight. Thus, the catalytic performance of all catalysts was compared at different reaction temperatures. The ethanol dehydration activity is apparently significant at ca. 200 °C and total at 400 °C as established in Figures 5a,b and 6a,b. In Figure 5a, ethanol conversion increases with the increasing reaction temperature because of the enhanced reaction rate as well as the nature of the endothermic reaction. The obtained catalytic activity of all catalysts was the highest at 400 °C without deactivation. For the bare Al_2O_3 catalyst, the ethanol conversion is extremely high, from 3.3 to 72.0%, despite the absence of modification with other metals. This is consistent with our previous works[24,45] described that an increase in the ethanol conversion corresponded to the amount of lattice water on the surface,

https://doi.org/10.1021/acsomega.1c02818
ACS Omega 2021, 6, 19911−19923

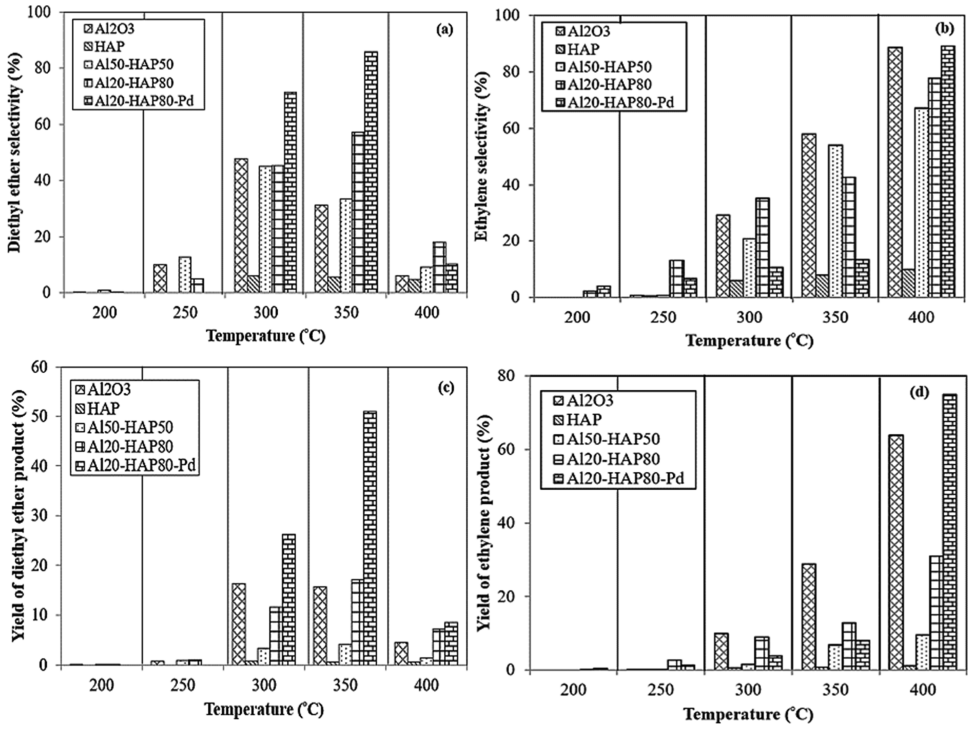

Figure 6. Selectivity of diethyl ether and ethylene (a,b) and yield (c,d) of all different catalysts, respectively. Reaction condition: 0.05 g catalyst, ethanol flow rate = 1.45 mL/h, at atmospheric pressure, WHSV = 22.9 ($g_{ethanol}$ g_{cat}^{-1}) h^{-1}.

which was evaluated from the Al 2p and O 1s peaks from the XPS technique. The quantities of lattice water are significantly high in the bare Al_2O_3 catalyst, hence leading to effective ethanol dehydration. For bare HAP and Al50-HAP50 catalysts, low ethanol conversions were observed over the whole reaction temperature (1.3 to 13.0% for HAP and 4.6 to 14.3% for Al50-HAP50). The deterioration of ethanol conversion can be ascribed to the lower amount of weak acid sites. In the case of increasing the ratio of HAP from 50 to 80% or Al20-HAP80, this catalyst showed a mild increasing trend in ethanol conversion with reaction temperature as indicated by the ethanol conversion of 40.0% at 400 °C. The quantification of the Al20-HAP80 catalyst exhibited higher weak acid sites than those of the Al50-HAP50 catalyst. The specific interaction between the surface hydroxyls of Al_2O_3 (acidity) and basicity of HAP in that Al_2O_3−HAP catalysts were explained by the presence of surface acid sites, especially weak acid sites (Lewis acid sites), resulting thus in enhanced catalytic activity.[46] Obviously, the amount of the HAP exerts a significant effect on the ethanol dehydration. In addition, we extend our study on how the Pd (0.5 wt %) modified on the Al20-HAP80 catalyst affects the catalytic activity. Consequently, the Al20-HAP80-Pd catalyst shows an improvement in catalytic activity by raising the reaction temperature, where the ethanol conversion reaches its maximum value of 84.2% at 400 °C. According to the rate of reaction and/or ethanol consumption rate (Figure 5 b), it was found that the reaction rate of each catalyst was increased with an increase in the reaction temperature. Moreover, the reaction rate was found to be enhanced when modifying the Al20-HAP80 catalyst with Pd. This can be ascribed to the presented Al_2O_3−HAP that is surrounded by the Pd sites, which would significantly improve the catalytic activity. Yang and Nakane[47] have shown that the catalytic sites of Pd and specific active oxygen species (surface anion radicals O^- and surface superoxide anions O_2) are formed that favor catalytic activity in ethanol dehydration. Notably, the Al20-HAP80-Pd catalyst exhibited the highest reaction rates of 190.04 mol ethanol·g_{cat}^{-1}·h^{-1} at 400 °C among all different catalysts. These results agree well with ethanol conversion results. It should be noted that this result was related to acidity of catalysts as proved in NH_3-TPD results. Thus, the acidity of the catalysts is a key factor to improve the catalytic activity.

The product selectivity of all different catalysts is shown in Figure 6a,b. It revealed that low reaction temperatures (200−350 °C) are favorable to diethyl ether formation by intermolecular dehydration, whereas high reaction temperatures (ca. >350 °C) are favorable to ethylene formation by intramolecular dehydration. At low reaction temperatures, not only the catalyst activity is poor but also the selectivity of ethylene is low because of a large amount of ethanol being transformed to diethyl ether.[48] The minor undesired product was acetaldehyde, which is also produced by ethanol dehydrogenation as a side reaction (refers Table S1 under Supporting Information). The bare Al_2O_3 catalyst predominantly leads to the high diethyl ether selectivity (ca. 47.8%) at 350 °C and high ethylene selectivity (ca. 88.6%) at 400 °C; thus, this catalyst is considered to be a typical strong acid catalyst, while the coke formation (3.41 wt %, not shown data) was of a major effect under the investigated reaction condition. In contrast, low diethyl ether selectivity (ca. 0.0−4.7%) and low ethylene selectivity (ca. 0.0−10.0%) were obtained from the bare HAP catalyst, which is a typical basic catalyst. So, we hypothesized that addition of the HAP catalyst (basic catalyst) into the Al_2O_3 catalyst (strong acid catalyst) can produce high selectivity of diethyl ether and ethylene with suitable reaction conditions. By modifying Al_2O_3 with HAP, the highest diethyl ether selectivity (ca. 57.1%) was found over the Al20-HAP80 catalyst at 350 °C. Nevertheless, the diethyl ether selectivity decreased due to its decomposition to ethylene at high reaction temperature. The selectivity of ethylene appears to have a

https://doi.org/10.1021/acsomega.1c02818
ACS Omega 2021, 6, 19911−19923

Scheme 2. Mechanism of Catalytic Ethanol Dehydration to Ethylene (a) and Diethyl Ether (b) Over Al_2O_3−HAP Catalyst with Pd Modification

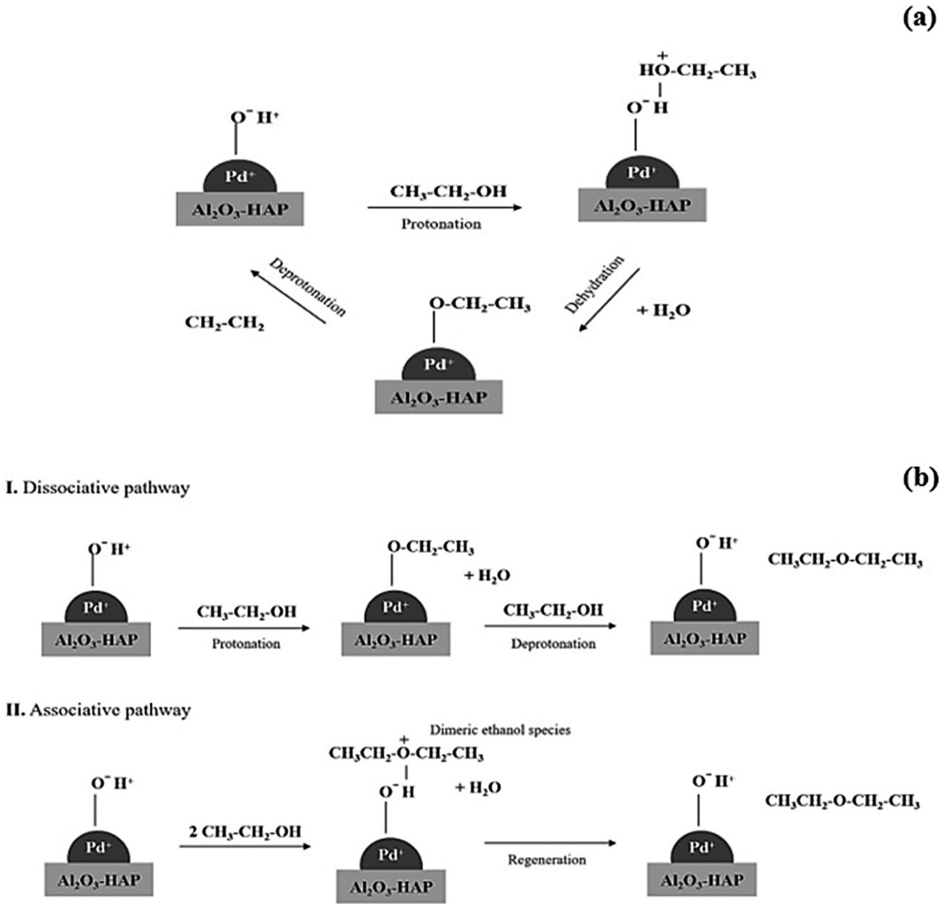

maximum value of 77.7% at 400 °C when compared to the results of the Al50-HAP50 catalyst. After the modification of the active Pd (0.5 wt %) on the Al20-HAP80 catalyst, the results show a relatively outstanding catalytic performance with respect to the other catalysts. The diethyl ether selectivity gives a maximum value of 85.9% at 350 °C. However, when the reaction temperature was increased to 400 °C, agreeing with the endothermic nature of intramolecular dehydration, ethylene is the main product. The Al20-HAP80-Pd catalyst has enriched weak acid sites (312.7 μmol NH_3 g^{-1} cat.), which conceivably renders its superior ethylene selectivity of 89.1%. The positive effect of weak acid sites (Lewis acid sites) on diethyl ether and ethylene production has been similarly demonstrated in the work of Tresatayawed et al.[25] In addition, the catalytic sites of noble palladium oxide is also very important to activate and dissociate the first C−H bond of ethanol molecules that is the rate-determining step of ethanol dehydration.[49] Besides, the highest acid density of weak acid sites of Al20-HAP80-Pd catalyst (100.9 μmol m^{-2}, Table 2) might be the crucial aspects to improve the catalytic performance in ethanol dehydration. Also, higher acid density and the distance between the electronegativity (the more electronegative, the more acidic) of the noble Pd (2.2) and Al_2O_3−HAP catalyst [EN of $(Al):(Ca)_{HAP}$ = (1.61):(1.0)] may be the factors which allow the ethanol molecules easily adsorbed and rapidly catalyzed to produce the main product, especially diethyl ether and ethylene.[45] Feng et al.[50] claimed that the generated weak acid sites and reduced strong acid sites may be ascribed to the synergistic action between weak electronegativity compared to the strong electronegativity, which is associated with increasing the product selectivity.

The diethyl ether and ethylene yields (calculated by multiplying the selectivity of the product by the conversion of ethanol) are shown in Figure 6c,d. From all different catalysts, the Al20-HAP80-Pd catalyst gives excellent results in producing diethyl ether yield (51.0% at 350 °C) and ethylene yield (75.0% at 400 °C) due to the high amount of weak acid sites in terms of weak acid density. In addition, it is noticed that the Pd modification on the catalysts affected the product yield by merely increasing the acetaldehyde yield in temperature range of 200−250 °C (refers Table S2 under Supporting Information), which could be consistent with the phenomenon of the Pd site on γ-Al_2O_3−P as reported in our previous work.[24] Thus, the acidic properties and nature of surface catalysts are important and effective to the catalytic performance in dehydration of ethanol to form diethyl ether and ethylene. It is recognized that the dehydration of ethanol essentially takes place on Lewis acid sites (weak acid sites).[51] Besides surface acid sites, the textural properties of alumina/hydroxyapatite catalysts could also affect the ethanol conversion and product selectivity as well as product yield. Our data and our explanation agree with the data reported by Cheng et al.[52] that found the catalysts with low BET surface area and pore volume can improve the ethylene selectivity from ethanol dehydration due to plausible hindrance of the multiple adsorption of ethanol molecules, thereby decreasing

https://doi.org/10.1021/acsomega.1c02818
ACS Omega 2021, 6, 19911−19923

the possibility of side reactions. Hence, the Al20-HAP80-Pd catalyst represents the outstanding catalytic performance in dehydration of ethanol to diethyl ether and ethylene at suitable reaction conditions, attributed to its highest weak acid sites (refers to Lewis acid sites), small amount of strong acid sites, and reasonably lower textural properties.

Understanding the detail in reaction mechanisms of ethanol dehydration to ethylene and diethyl ether would be of particular interest to justify the results and, what is more important, be able to design an improved catalytic system. As shown in Scheme 2a, the ethanol molecule is attracted to the Brønsted acid site, where the proton is transferred to the ethanol hydroxyl group (proton transfers from acid to oxygen atom to form alkyloxonium ion), which subsequently releases water molecules to form an intermediate.[41] Water molecules function as Brønsted acid capable of releasing proton since the OH bond is weakened during adsorption onto the Lewis acid site of Al−HAP−Pd^{+}−O. Afterward, an ethoxide surface group forms and deprotonates one hydrogen atom of the methyl group to form ethylene. Under this mechanistic scheme, the formation of ethylene is mainly ascribed to a higher density of Lewis acid sites, which results from Al−HAP−Pd^{+}−O groups on the catalyst surface. Thus, the reaction mechanism involves adjacent Lewis acid sites playing a vital role in enhancing the catalytic activity and selectivity to ethylene. Besides, Sarve et al.,[41] reported that some of the ethylene molecules adsorbed on Lewis acid sites and metallic sites of the Al20-HAP80-Pd catalyst act as an intermediate for diethyl ether. According to the research works,[25,53,54] the dehydration of ethanol to diethyl ether is represented by two different pathways, termed the dissociative pathway and associative pathway (Scheme 2b). The dissociative pathway occurs by one ethanol molecule adsorbed on the catalyst and followed by water molecule elimination to obtain the adsorbed ethoxide. Subsequently, the ethoxide on the surface catalyst reacts with the second ethanol molecule on an adjacent-framework oxygen to produce diethyl ether. In the associative pathway, an ethanol molecule is adsorbed at a proton site; then, by the adsorption of another ethanol molecule in close vicinity, the dimeric ethanol species are formed. In the dimeric intermediate, the proton is held between the alcohol oxygen atoms. Later, protonated dimers rearrange and decompose into water molecules and an adsorbed diethyl ether, which desorbs to regenerate the proton site. Also, the noble metal of Pd was proposed to influence the adjacent Lewis acid sites on the surface of the Al20-HAP80-Pd catalyst, and a significant amount of diethyl ether was generated.[55] Concerning the ethanol dehydration reaction, the formation of diethyl ether at low reaction temperature might be the intermediate in the formation of ethylene at high reaction temperature. Therefore, the high main product (diethyl ether and ethylene) selectivity and/or yield in our present work can be related to the weak acid sites (Lewis acid sites) as well as the reduction of strong acid sites. Despite these promising results, however, further enhancements in catalytic performance and the development of reaction conditions are still required.

After the activity test, the Al20-HAP80-Pd catalyst was chosen to further explore the catalyst stability by carrying out a short (10 h) time-on-stream (TOS) experiments at suitable reaction conditions (ca. 350 °C for diethyl ether yield and ca. 400 °C for ethylene yield), and the result is presented in Figure 7. At the low reaction temperature, that is ca. 350 °C, the diethyl ether yield was relatively stable at about 51.9−55.4%.

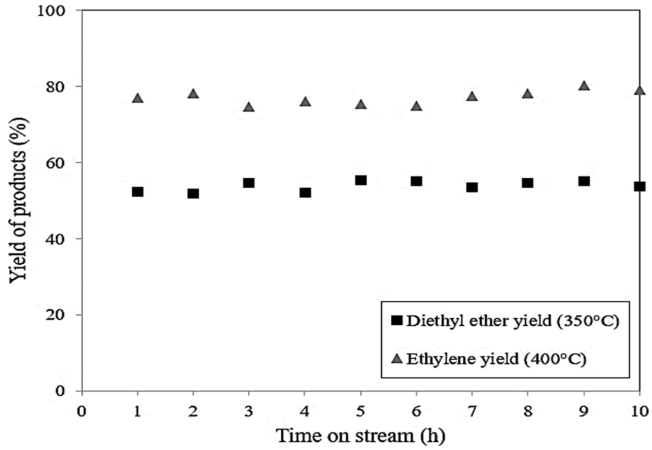

Figure 7. Stability test for the Al20-HAP80-Pd catalyst under the investigate reaction for 10 h.

At the high reaction temperature, that is ca. 400 °C, the ethylene yield was comparatively stable at about 74.7−80.2% throughout TOS. These results indicate that the Al20-HAP80-Pd catalyst has a high catalytic activity and high stability in ethanol dehydration for the production of diethyl ether and ethylene. According to Chen et al.,[56] the incorporation of Pd into the lattice of Al_2O_3−HAP catalyst and displaces the Al_2O_3−HAP (calcium aluminate ion) sites to form [Al−HAP]−Pd^{+}−O bonds, which increase the negative charge around the Al_2O_3−HAP. As a result, the interaction between Pd species and the Al_2O_3−HAP is enhanced, leading to the improvement of the thermal stability, we think which may be one reason for the good stability of the Al20-HAP80-Pd catalyst.

Thermal analysis was performed to study coke deposit on the spent catalyst from TOS for 10 h. For the temperature range of 200−800 °C, the weight loss during this period is due to the de-coking process and three distinct stages are observed (Figure 8). The first stage of the weight loss at the temperature

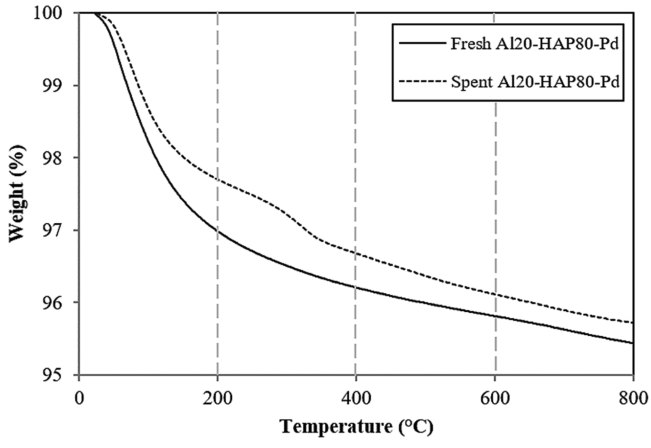

Figure 8. TGA curve of the fresh and spent Al20-HAP80-Pd catalysts.

range of 200−400 °C is referred to soft coke. As the temperature increases from 400 to 600 °C, the second stage is called hard coke. This shows that the coke deposit on the spent catalyst is hard coke which can be removed with proper de-coking methods.[57] From 600 to 800 °C (third stage), reaction rate declines and is called laid coke, either due to its non-

https://doi.org/10.1021/acsomega.1c02818
ACS Omega 2021, 6, 19911−19923

Table 3. Comparison of Different Catalysts for Ethanol Dehydration to Diethyl Ether and Ethylene in this Work and Others

catalysts	reaction conditions	diethyl ether yield (%)	ethylene yield (%)	references
Al20-HAP80-Pd	200−400 °C, 1 atm and (WHSV 22.9 h^{-1})	51.0 (at 350 °C)	75.0 (at 400 °C)	this work
0.5Pd/Al_2O_3−P	200−400 °C, 1 atm and (WHSV 22.9 h^{-1})	33.3 (at 350 °C)	43.7 (at 400 °C)	24
Pd-HBZ-N	200−400 °C, 1 atm and (WHSV 22.9 h^{-1})	48.0 (at 250 °C)	99.0 (at 400 °C)	58
PdW/TiO_2	200−400 °C, 1 atm and (WHSV 3.13 h^{-1})	41.4 (at 300 °C)	63.2 (at 400 °C)	25
Pd-G-Al	200−400 °C, 1 atm and (WHSV 22.9 h^{-1})	34.0 (at 350 °C)	80.0 (at 400 °C)	59
Pd(II)-doped SiO_2/Fe_2O_3	280−670 °C, 1 atm	n.a.[a]	15.3 (at 670 °C)	47
$AlPO_4$/HAP	340 °C, 200 bar and (WHSV 1.01 h^{-1})	75.0	n.a.[a]	19

[a]n.a. not analysed.

reactivity or difficulty of left-over coke deep in the catalyst particles. However, initial weight loss up to 200 °C is supposed to be due to the removal of water molecules and volatile materials; therefore, it had no effect on the coke calculation. Thus, we could probably claim that at a temperature above 400 °C in TG profiles included hard and laid cokes on the spent catalysts. We calculated the coke formation on the Al20-HAP80-Pd catalyst surface in the temperature range of 400−800 °C. Therefore, we found that the weight losses of the fresh and spent Al20-HAP80-Pd catalysts in this stage were insignificantly different, showing less amount of coke formation. The quantitative calculation results demonstrated that the weight loss of the spent catalyst was about 1.98%.

Table 3 shows a comparison between the Al20-HAP80-Pd catalyst in this study and those reported in the literature. However, the diethyl ether yield and ethylene yield over the Al20-HAP80-Pd catalyst is not relatively high compared to some catalysts. Finally, it should be emphasized that, apart from their interesting intrinsic activity, the Al20-HAP80-Pd tested in this study was a highly stable catalyst under mild and green reaction conditions, thus making them have potential to be applied in an industrial scale ethanol to diethyl ether and ethylene plants competitive with steam cracking plants.

3. CONCLUSIONS

In this work, the study of ethanol dehydration, under the gas phase from the temperature range of 200−400 °C, over different composition ratios of Al_2O_3−HAP catalysts has been thoroughly investigated for the first time. In addition, the modification of Pd (0.5 wt %) on the optimal ratio of the Al_2O_3−HAP catalyst was evaluated. These results show that the acidic sites present and their strengths have been related with the catalytic activities and the respective selectivities to diethyl ether and ethylene. The combination of Al_2O_3−HAP catalysts with a suitable ratio generated significant amounts of weak acid sites and reduced strong acid sites, which is considered to be relatively favorable for catalytic performance. Deposition of Pd on the Al20-HAP80 catalyst led to an extreme increase in the amount of weak acid sites (312.7 μmol NH_3 g^{-1} cat.) as well as weak acid density (100.9 μmol m^{-2}) due to the presence of Al_2O_3−HAP (calcium aluminate ion and/or bonds) that is surrounded by the Pd sites; the catalytic activity can be facilitated. In particular, the Al20-HAP80-Pd catalyst showed the best performance in term of diethyl ether yield (ca. 51.0%) at a reaction temperature of 350 °C, whereas 75.0% yield of ethylene was observed at a higher reaction temperature of 400 °C. The stability of the catalyst was confirmed by TOS for 10 h without a deactivation trend and significant evidence of coke deposition. Therefore, it can be concluded that the catalytic performance of our catalysts may be assigned to a combination of weak acid sites (Lewis acidity), small amount of strong acid sites, and structural characteristics of the catalytic materials used. Nevertheless, our further work is still required in order to develop the ambiguities of the surface of the solid acid catalysts.

4. EXPERIMENTAL SECTION

4.1. Materials. Commercial gamma alumina from BASF Company, hydroxyapatite-nanopowder ([$Ca_5(OH)(PO_4)_3$, HAP], CAS: 12167-74-7, Sigma-Aldrich company, USA), tetraamminepalladium(II) nitrate ($Pd(NO_3)_2{\cdot}4NH_3$, Sigma-Aldrich company, USA as a precursor), and toluene (ACS reagent, 99.7%, Sigma-Aldrich company, USA) were used as received without further treatment and were used in the present investigation.

4.2. Catalyst Preparation. Initially, alumina (Al_2O_3) nanoparticles were mixed with hydroxyapatite (HAP) by the physical mixing method in toluene and stirred at room temperature for 40 min to achieve good homogeneity. Then, the solvent was removed from the mixture and washed by deionized water. The obtained Al_2O_3−HAP catalysts were dried in an oven at 110 °C overnight and further calcined in synthetic air at 600 °C for 2 h with a heating rate of 10 °C min^{-1}. After calcination, we placed the catalyst in a sample bottle and maintained the bottle at room temperature. In our present work, different weight ratios of Al_2O_3−HAP (1:0, 0:1, 5:5 and 2:8) were prepared and denoted as Al_2O_3, HAP, Al50-HAP50, and Al20-HAP80, respectively.

To investigate the effect of Pd modification on the optimal catalyst, the best composition ratio of the Al_2O_3−HAP catalyst having the highest catalytic activity was prepared by incipient wetness impregnation using an aqueous solution of tetraamminepalladium(II) nitrate as the Pd precursor (nominal palladium content of 0.5 wt %). The catalyst was dried in an oven at 110 °C overnight and calcined in synthetic air at 600 °C for 6 h (heating rate of 10 °C min^{-1}). The catalyst was then cooled to room temperature and ground for physicochemical characterization and reaction studies. The impregnated catalyst is denoted as Al20-HAP80-Pd.

4.3. Catalyst Characterization. *4.3.1. X-ray Powder Diffraction.* XRD patterns of catalysts powders were determined in a 2θ ranges from 10° to 80° at a scan rate of 1.5° min^{-1} from a Bruker D8 ADVANCE X-ray diffractometer using the Cu K_α radiation source (λ = 0.15418 nm) as the X-ray source. The phases were identified using JCPDS (Joint committee on powder diffraction standards) powder diffraction files.

4.3.2. Nitrogen Physisorption. BET surface area and porosity were performed by using N_2 isothermal sorption measurements at −196 °C and were determined volumetrically with a Micromeritics ASAP 2020 instrument (Micromeritics Instrument Corp., USA). The catalyst was thermally heated at

https://doi.org/10.1021/acsomega.1c02818
ACS Omega 2021, 6, 19911−19923

200 °C for 4 h before the nitrogen physisorption process. The total surface area of the catalyst was calculated using the BET isotherm method, while the pore volume and average pore size were estimated using the BJH correlation.

4.3.3. Inductively Coupled Plasma. The catalysts were measured by the PerkinElmer OPTIMA 2000TM instrument. In order to perform ICP analysis on the catalysts, a small amount of the deposit catalyst (~0.1 g) was dissolved in an appropriate acid mixture. Generally, most deposit catalysts can be dissolved in 10 mL of concentrated nitric/hydrochloric acid solution. Acid digestion may also be used; however, precaution must be taken to prevent loss of elements during the heating process. Before sample analysis, the ICP must be calibrated. Calibration consists of analyzing standards and a blank within the linear range of the element being analyzed.

4.3.4. SEM and EDX. The morphologies of the catalysts were determined by the JEOL mode JSM-5800LV scanning electron microscope, and the elemental distribution over the catalysts surface was determined by Link Isis Series 300 program EDX operated at 100 kV. Micrographs were taken at an accelerating voltage of 30 kV and magnification ranged between 1000 and 10,000 and a resolution of 3 nm.

4.3.5. Ammonia Temperature-Programmed Desorption. The acidity and acid strength of all catalysts were determined by using a Micromeritics Chemisorp 2750 Pulse for temperature-programmed desorption of ammonia. In the experiment, 0.03 g of quartz wool and 0.1 g of catalyst were loaded in a U-tube glass, and then, the catalyst was pretreated at 450 °C in a flow of He for 1 h (He flow rate of 25 cm^3 min^{-1}). After the temperature cooled down to 40 °C, the catalyst was saturated with 15% NH_3/He for 30 min. After that, the excess adsorbed gas (physisorbed) NH_3 was purged with He until the base line was constant. Subsequently, the desorption of NH_3 was conducted by an increase of temperature from 40 to 600 °C with a heating rate of 10 °C min^{-1}.

4.3.6. Thermogravimetric Analysis. The thermal decomposition of fresh/spent catalysts were carried out from ambient temperature to 800 °C with a heating rate of 10 °C min^{-1} under N_2 atmosphere using a STD Analyzer model Q600 from TA instrument (USA).

4.4. Catalytic Testing. *4.4.1. Temperature-Programmed Reaction.* Catalytic experiments were performed at atmospheric pressure in a fixed-bed continuous flow micro-reactor (i.d. 7 mm). The temperature was measured using a microprocessor-based temperature controller through a K-type thermocouple reaching the top of the catalyst bed. In each experiment, 0.05 g of catalyst particles and 0.01 g of quartz wool were packed in the middle of reactor, which is located in an electrically heated furnace. The pretreatment was performed in a flow system operated under purified N_2 gas with 50 mL min^{-1} at 200 °C for 1 h to eliminate any trace of water from the catalyst. Then, ethanol (conc. 99.98%) was vaporized and injected into the reactor by using a single syringe pump at total flow rate of 1.45 mL h^{-1}. The WHSV of ethanol was set at a selected value of 22.9 ($g_{ethanol}$ g_{cat}^{-1}) h^{-1}. Finally, all products were quantified in a reaction temperature ranging from 200 to 400 °C under atmospheric pressure. The reaction was kept for 1 h to reach a steady-state for each reaction temperature. The outlet gases were analyzed by a Shimadzu (GC-14B) gas chromatograph with a flame ionization detector (FID) using capillary column (DB-5). GC signals were quantified by proper calibration standards. The catalytic performance was reported in terms of ethanol conversion (X_{EtOH}, in %), product selectivity (S_i, in %), product yields (Y_i, in %), and rate of reaction (v_{rxn}, in moles of ethanol per gram of catalyst per hour), which are computable via eqs 1−4:

$$X_{EtOH}(\%) = \frac{n_{EtOH}(in) - n_{EtOH}(out)}{n_{EtOH}(in)} \times 100 \quad (1)$$

$$S_i(\%) = \frac{n_i}{\sum n_i} \times 100 \quad (2)$$

$$Y_i(\%) = \frac{X_{EtOH} \times S_i}{100} \quad (3)$$

$$v_{rxn} = \frac{v_{feed} X_{EtOH}}{RTm_{cat}} \quad (4)$$

where $n_{EtOH}(in)$ is the number of moles of ethanol in the feed, $n_{EtOH}(out)$ is the number of moles of unreacted ethanol, n_i is the number of moles of product i, v_{feed} is the ethanol feed rate (in moles of ethanol per hour), R is the gas constant (0.0821 L atm/mol K), T is the studied temperature (in kelvins), and m_{cat} is the mass of catalyst used (in grams).

4.4.2. Stability Test. The best composition ratio of the Al_2O_3−HAP catalyst having the maximum catalytic activity in the temperature programmed reaction was selected to study its catalytic stability as a function of time on stream (TOS) at optimal reaction conditions by extending the time-on-stream duration to 10 h. The experiment was similar to those of temperature-programmed reaction testing as described above.

■ ASSOCIATED CONTENT

Supporting Information

The Supporting Information is available free of charge at https://pubs.acs.org/doi/10.1021/acsomega.1c02818.

Elemental mapping of the bare Al_2O_3 catalyst, bare HAP catalyst, Al50-HAP50 catalyst, and Al20-HAP80 catalyst, ethanol conversion of Al_2O_3, Al_2O_3−Pd, HAP, and HAP−Pd catalysts, selectivity of diethyl ether and ethylene of Al_2O_3, Al_2O_3−Pd, HAP, and HAP−Pd catalysts, ethanol conversion and product selectivity from ethanol dehydration at temperatures ranging from 200 to 400 °C, and product yield from ethanol dehydration at temperatures ranging from 200 to 400 °C (PDF)

■ AUTHOR INFORMATION

Corresponding Author

Bunjerd Jongsomjit − *Center of Excellence on Catalysis and Catalytic Reaction Engineering, Department of Chemical Engineering, Faculty of Engineering, Chulalongkorn University, Bangkok 10330, Thailand; Bio-Circular-Green-Economy Technology & Engineering Center, BCGeTEC, Department of Chemical Engineering, Faculty of Engineering, Chulalongkorn University, Bangkok 10330, Thailand;* orcid.org/0000-0002-9558-9190; Phone: +66-221-86874; Email: bunjerd.j@chula.ac.th; Fax: +66-221-86877

Authors

Chaowat Autthanit − *Center of Excellence on Catalysis and Catalytic Reaction Engineering, Department of Chemical Engineering, Faculty of Engineering, Chulalongkorn University, Bangkok 10330, Thailand; Bio-Circular-Green-Economy Technology & Engineering Center, BCGeTEC,*

Department of Chemical Engineering, Faculty of Engineering, Chulalongkorn University, Bangkok 10330, Thailand

Nutdanai Likitpiriya − *Center of Excellence on Catalysis and Catalytic Reaction Engineering, Department of Chemical Engineering, Faculty of Engineering, Chulalongkorn University, Bangkok 10330, Thailand*

Piyasan Praserthdam − *Center of Excellence on Catalysis and Catalytic Reaction Engineering, Department of Chemical Engineering, Faculty of Engineering, Chulalongkorn University, Bangkok 10330, Thailand;* orcid.org/0000-0001-8021-2115

Complete contact information is available at: https://pubs.acs.org/10.1021/acsomega.1c02818

Notes

The authors declare no competing financial interest.

■ ACKNOWLEDGMENTS

This research work is funded by Chulalongkorn University (under the Ratchadapisek Somphot and Fundamental Fund) and TSRI under the CAT-REAC industrial project. The authors also would like to thank the Ratchadapisek Somphot Fund for Postdoctoral Fellowship, Chulalongkorn University, for supporting this research.

■ REFERENCES

(1) Guzmán-Martínez, C. E.; Maya-Yescas, R.; Castro-Montoya, A. J.; Nápoles Rivera, F. Dynamic simulation of control systems for bioethanol reactive dehydration: Conventional and intensified case studies. *Chem. Eng. Process.* **2021**, *159*, 108238.

(2) Suerz, R.; Eränen, K.; Kumar, N.; Wärnå, J.; Russo, V.; Peurla, M.; Aho, A.; Yu Murzin, D.; Salmi, T. Application of microreactor technology to dehydration of bio-ethanol. *Chem. Eng. Sci.* **2021**, *229*, 116030.

(3) Li, J.; Chen, G.; Yan, J.; Huang, B.; Cheng, H.; Lou, Z.; Li, B. Solar-driven plasmonic tungsten oxides as catalyst enhancing ethanol dehydration for highly selective ethylene production. *Appl. Catal., B* **2020**, *264*, 118517.

(4) Kamsuwan, T.; Praserthdam, P.; Jongsomjit, B. Diethyl ether production during catalytic dehydration of ethanol over Ru-and Pt-modified H-beta zeolite catalysts. *J. Oleo Sci.* **2017**, *66*, 199−207.

(5) Zhang, M.; Yu, Y. Dehydration of ethanol to ethylene. *Ind. Eng. Chem. Res.* **2013**, *52*, 9505−9514.

(6) Chen, Y.; Wu, Y.; Tao, L.; Dai, B.; Yang, M.; Chen, Z.; Zhu, X. Dehydration reaction of bio-ethanol to ethylene over modified SAPO catalysts. *J. Ind. Eng. Chem.* **2010**, *16*, 717−722.

(7) Angelici, C.; Weckhuysen, B. M.; Bruijnincx, P. C. A. Chemocatalytic conversion of ethanol into butadiene and other bulk chemicals. *ChemSusChem* **2013**, *6*, 1595−1614.

(8) Fan, D.; Dai, D.-J.; Wu, H.-S. Ethylene formation by catalytic dehydration of ethanol with industrial considerations. *Materials* **2013**, *6*, 101−115.

(9) Garbarino, G.; Prasath Parameswari Vijayakumar, R.; Riani, P.; Finocchio, E.; Busca, G. Ethanol and diethyl ether catalytic conversion over commercial alumina and lanthanum-doped alumina: reaction paths, catalyst structure and coking. *Appl. Catal., B* **2018**, *236*, 490−500.

(10) Phung, T. K.; Busca, G. Ethanol dehydration on silica-aluminas: active sites and ethylene/diethyl ether selectivities. *Catal. Commun.* **2015**, *68*, 110−115.

(11) Chen, G.; Li, S.; Jiao, F.; Yuan, Q. Catalytic dehydration of bioethanol to ethylene over TiO_2/γ-Al_2O_3 catalysts in microchannel reactors. *Catal. Today* **2007**, *125*, 111−119.

(12) Bedia, J.; Barrionuevo, R.; Rodríguez-Mirasol, J.; Cordero, T. Ethanol dehydration to ethylene on acid carbon catalysts. *Appl. Catal., B* **2011**, *103*, 302−310.

(13) Phung, T. K.; Lagazzo, A.; Rivero Crespo, M. Á.; Sánchez Escribano, V.; Busca, G. A study of commercial transition aluminas and of their catalytic activity in the dehydration of ethanol. *J. Catal.* **2014**, *311*, 102−113.

(14) Doheim, M. M.; Hanafy, S. A.; El-Shobaky, G. A. Catalytic conversion of ethanol and isopropanol over the Mn_2O_3/Al_2O_3 system doped with Na_2O. *Mater. Lett.* **2002**, *55*, 304−311.

(15) Feng, R.; Hu, X.; Yan, X.; Yan, Z.; Rood, M. J. A high surface area mesoporous γ-Al_2O_3 with tailoring texture by glucose template for ethanol dehydration to ethylene. *Microporous Mesoporous Mater.* **2017**, *241*, 89−97.

(16) Tasbihi, M.; Feyzi, F.; Amlashi, M. A.; Abdullah, A. Z.; Mohamed, A. R. Effect of the addition of potassium and lithium in $Pt-Sn/Al_2O_3$ catalysts for the dehydrogenation of isobutane. *Fuel Process. Technol.* **2007**, *88*, 883−889.

(17) Lee, M.-H.; Nagaraja, B. M.; Natarajan, P.; Truong, N. T.; Lee, K. Y.; Yoon, S.; Jung, K.-D. Effect of potassium addition on bimetallic $PtSn/\theta$-Al_2O_3 catalyst for dehydrogenation of propane to propylene. *Res. Chem. Intermed.* **2016**, *42*, 123−140.

(18) He, S.; Sun, C.; Bai, Z.; Dai, X.; Wang, B. Dehydrogenation of long chain paraffins over supported $Pt-Sn-K/Al_2O_3$ catalysts: A study of the alumina support effect. *Appl. Catal., A* **2009**, *356*, 88−98.

(19) Rahmanian, A.; Ghaziaskar, H. S. Continuous dehydration of ethanol to diethyl ether over aluminum phosphate−hydroxyapatite catalyst under sub and supercritical condition. *J. Supercrit. Fluids* **2013**, *78*, 34−41.

(20) Ghantani, V. C.; Lomate, S. T.; Dongare, M. K.; Umbarkar, S. B. Catalytic dehydration of lactic acid to acrylic acid using calcium hydroxyapatite catalysts. *Green Chem.* **2013**, *15*, 1211−1217.

(21) Yan, B.; Tao, L.-Z.; Liang, Y.; Xu, B.-Q. Sustainable production of acrylic acid: catalytic performance of hydroxyapatites for gas-phase dehydration of lactic acid. *ACS Catal.* **2014**, *4*, 1931−1943.

(22) Tsuchida, T.; Sakuma, S.; Takeguchi, T.; Ueda, W. Direct synthesis of n-butanol from ethanol over nonstoichiometric hydroxyapatite. *Ind. Eng. Chem. Res.* **2006**, *45*, 8634−8642.

(23) Tsuchida, T.; Yoshioka, T.; Sakuma, S.; Takeguchi, T.; Ueda, W. Synthesis of biogasoline from ethanol over hydroxyapatite catalyst. *Ind. Eng. Chem. Res.* **2008**, *47*, 1443−1452.

(24) Autthanit, C.; Khaochartchai, C.; Praserthdam, P.; Jongsomjit, B. Elucidation of Pd modification effect on catalytic behaviors of γ-Al_2O_3-P catalysts toward ethanol dehydration and dehydrogenation. *Catal. Commun.* **2021**, *148*, 106169.

(25) Tresatayawed, A.; Glinrun, P.; Autthanit, C.; Jongsomjit, B. Pd Modification and Supporting Effects on Catalytic Dehydration of Ethanol to Ethylene and Diethyl Ether over W/TiO_2 Catalysts. *J. Oleo Sci.* **2020**, *69*, 503−515.

(26) Bamdadi, M.; Bozorg, A.; Tavasoli, A.; Shateri, S.; Andache, M. Synthesis of Meso/Macroporous γ-Alumina via Aluminum Pellet with Controllable Porosity: Ammonium Bicarbonate Influences through Drying and Calcination Steps. *ChemistrySelect* **2019**, *4*, 5872−5879.

(27) Bouropoulos, N.; Stampolakis, A.; Mouzakis, D. E. Dynamic mechanical properties of calcium alginate-hydroxyapatite nano-composite hydrogels. *Sci. Adv. Mater.* **2010**, *2*, 239−242.

(28) De, M.; Gupta, S. P. S. Lattice imperfection studies in polycrystalline materials by x-ray diffraction line-profile analysis. *Pramana* **1984**, *23*, 721−744.

(29) Rabiei, M.; Palevicius, A.; Monshi, A.; Nasiri, S.; Vilkauskas, A.; Janusas, G. Comparing methods for calculating nano crystal size of natural hydroxyapatite using X-Ray diffraction. *Nanomaterials* **2020**, *10*, 1627.

(30) Liu, D.; Lau, R.; Borgna, A.; Yang, Y. Carbon dioxide reforming of methane to synthesis gas over Ni-MCM-41 catalysts. *Appl. Catal., A* **2009**, *358*, 110−118.

(31) Charmas, B.; Skubiszewska-Zięba, J.; Kucio, K.; Skwarek, E. Influence of mechanochemical treatment on thermal and structural properties of silica−collagen and hydroxyapatite−collagen composites. *Adsorption* **2019**, *25*, 591−599.

(32) El Shafei, G. M. S.; Philip, C. A.; Moussa, N. A. Fractal analysis of hydroxyapatite from nitrogen isotherms. *J. Colloid Interface Sci.* **2004**, *277*, 410−416.
(33) de Lima, M. G.; Leal, E.; Agnolon Pallone, E. M. d. J.; Kiminami, R. H. G. A.; Costa, A. C. F. d. M. Microstructural and Mechanical Properties of Al2O3/HAp Composites for Use as Bone Substitute Material. *Mater. Sci. Forum.* **2018**, *912*, 153−158.
(34) Gopi, D.; Shinyjoy, E.; Karthika, A.; Nithiya, S.; Kavitha, L.; Rajeswari, D.; Tang, T. Single walled carbon nanotubes reinforced mineralized hydroxyapatite composite coatings on titanium for improved biocompatible implant applications. *RSC Adv.* **2015**, *5*, 36766−36778.
(35) Einhäuser, T. J. ICP-OES and SEM-EDX analysis of dust and powder produced by the laser-processing of a Cr-Ni-steel alloy. *Microchim. Acta* **1997**, *127*, 265−268.
(36) Lei, S.; Zhang, Z.-h.; Qiu, Z.-g.; Fang, G.; Zhang, W.; Zhao, L.-f. Effect of phosphorus modification on the catalytic properties of Mo-Ni/Al_2O_3 in the hydrodenitrogenation of coal tar. *J. Fuel Chem. Technol.* **2015**, *43*, 74−80.
(37) Zhao, R.; Lu, P.; Zhao, Y.; Zhang, L.; Zhao, Y.; Yang, C.; Liu, C.; Liu, D. Effect of Phosphorus Modification on the Acidity, Nanostructure of the Active Phase, and Catalytic Performance of Residue Hydrodenitrogenation Catalysts. *ACS Omega* **2020**, *5*, 19111−19119.
(38) Samudrala, S. P.; Kandasamy, S.; Bhattacharya, S. Turning biodiesel waste glycerol into 1, 3-Propanediol: catalytic performance of sulphuric acid-activated montmorillonite supported platinum catalysts in glycerol hydrogenolysis. *Sci. Rep.* **2018**, *8*, 7484.
(39) Gao, J.; Fan, G.; Yang, L.; Cao, X.; Zhang, P.; Li, F. Oxidative esterification of methacrolein to methyl methacrylate over gold nanoparticles on hydroxyapatite. *ChemCatChem* **2017**, *9*, 1230−1241.
(40) Tavassoli, H.; Javadpour, J.; Taheri, M.; Mehrjou, M.; Koushki, N.; Arianpour, F.; Majidi, M.; Izadi-Mobarakeh, J.; Negahdari, B.; Chan, P.; Ebrahimi Warkiani, M.; Bonakdar, S. Incorporation of nanoalumina improves mechanical properties and osteogenesis of hydroxyapatite bioceramics. *ACS Biomater. Sci. Eng.* **2018**, *4*, 1324−1336.
(41) Sarve, D. T.; Singh, S. K.; Ekhe, J. D. Kinetic and mechanistic study of ethanol dehydration to diethyl ether over Ni-ZSM-5 in a closed batch reactor. *React. Kinet., Mech. Catal.* **2020**, *131*, 261−281.
(42) Khamkeaw, A.; Asavamongkolkul, T.; Perngyai, T.; Jongsomjit, B.; Phisalaphong, M. Interconnected Micro, Meso, and Macro Porous Activated Carbon from Bacterial Nanocellulose for Superior Adsorption Properties and Effective Catalytic Performance. *Molecules* **2020**, *25*, 4063.
(43) Corma, A.; Martinez, A.; Martinez, C. Isobutane/2-butene alkylation on ultrastable Y zeolites: Influence of zeolite unit cell size. *J. Catal.* **1994**, *146*, 185−192.
(44) Zhang, X.; Wang, R.; Yang, X.; Zhang, F. Comparison of four catalysts in the catalytic dehydration of ethanol to ethylene. *Microporous Mesoporous Mater.* **2008**, *116*, 210−215.
(45) Janlamool, J.; Jongsomjit, B. Catalytic ethanol dehydration to ethylene over nanocrystalline χ-and γ-Al_2O_3 catalysts. *J. Oleo Sci.* **2017**, *66*, 1029−1039.
(46) Ibrahim, M.; Labaki, M.; Giraudon, J.-M.; Lamonier, J.-F. Hydroxyapatite, a multifunctional material for air, water and soil pollution control: A review. *J. Hazard. Mater.* **2020**, *383*, 121139.
(47) Yang, H.; Nakane, K. Pd (II)-doped SiO_2/Fe_2O_3 nanofibers as a novel catalyst for the ethanol dehydration reaction. *J. Mater. Sci.* **2019**, *54*, 14763−14777.
(48) Wu, C.-Y.; Wu, H.-S. Ethylene formation from ethanol dehydration using ZSM-5 catalyst. *ACS Omega* **2017**, *2*, 4287−4296.
(49) Du, J.; Li, H.; Wang, C.; Zhang, A.; Zhao, Y.; Luo, Y. Improved catalytic activity over P-doped ceria-zirconia-alumina supported palladium catalysts for methane oxidation. *Catal. Commun.* **2020**, *141*, 106012.
(50) Feng, R.; Liu, S.; Bai, P.; Qiao, K.; Wang, Y.; Al-Megren, H. A.; Rood, M. J.; Yan, Z. Preparation and characterization of γ-Al_2O_3 with rich Brønsted acid sites and its application in the fluid catalytic cracking process. *J. Phys. Chem. C* . **2014**, *118*, 6226−6234.
(51) Nash, C. P.; Anand, R.; Danial, R.; Mayank, B.; Erica, G.; Micheal, G.; Hongda, Z.; Bala, S.; Joshua, S. Mixed alcohol dehydration over Brønsted and Lewis acidic catalysts. *Appl. Catal., A* **2016**, 110−124.
(52) Cheng, Y. W.; Chong, C. C.; Cheng, C. K.; Ng, K. H.; Witoon, T.; Juan, J. C. Ethylene production from ethanol dehydration over mesoporous SBA-15 catalyst derived from palm oil clinker waste. *J. Cleaner Prod.* **2020**, *249*, 119323.
(53) Phung, T. K.; Busca, G. Diethyl ether cracking and ethanol dehydration: acid catalysis and reaction paths. *Chem. Eng. J.* **2015**, *272*, 92−101.
(54) Gołąbek, K.; Tabor, E.; Pashkova, V.; Dedecek, J.; Tarach, K.; Góra-Marek, K. The proximity of aluminium atoms influences the reaction pathway of ethanol transformation over zeolite ZSM-5. *Commun. Chem.* **2020**, *3*, 25.
(55) Wu, X.; Fang, G.; Tong, Y.; Jiang, D.; Liang, Z.; Leng, W.; Liu, L.; Tu, P.; Wang, H.; Ni, J.; Li, X. Catalytic upgrading of ethanol to n-butanol: progress in catalyst development. *ChemSusChem* **2018**, *11*, 71−85.
(56) Chen, B.; Lin, J.; Chen, X.; Chen, Y.; Xu, Y.; Wang, Z.; Zhang, W.; Zheng, Y. Cooperative Catalysis of Methane Oxidation through Modulating the Stabilization of PdO and Electronic Properties over Ti-Doped Alumina-Supported Palladium Catalysts. *ACS Omega* **2019**, *4*, 18582−18592.
(57) Ahmed, R.; Sinnathamb, C. M.; Subbarao, D.; Subbarao, D. Kinetics of de-coking of spent reforming catalyst. *J. Appl. Sci.* **2011**, *11*, 1225−1230.
(58) Kamsuwan, T.; Jongsomjit, B. Characterization of different Si- and Al-based catalysts with Pd modification and their use for catalytic dehydration of ethanol. *J. Oleo Sci.* **2018**, *67*, 1005−1014.
(59) Kamsuwan, T.; Praserthdam, P.; Jongsomjit, B. Tuning of catalytic behaviors in ethanol dehydration with oxygen cofeeding over Pd-HBZ catalyst for ethylene production at low temperature. *Catal. Commun.* **2020**, *137*, 105941.

https://doi.org/10.1021/acsomega.1c02818
ACS Omega 2021, 6, 19911−19923